Journal of Materials Chemistry A

Accepted Manuscript

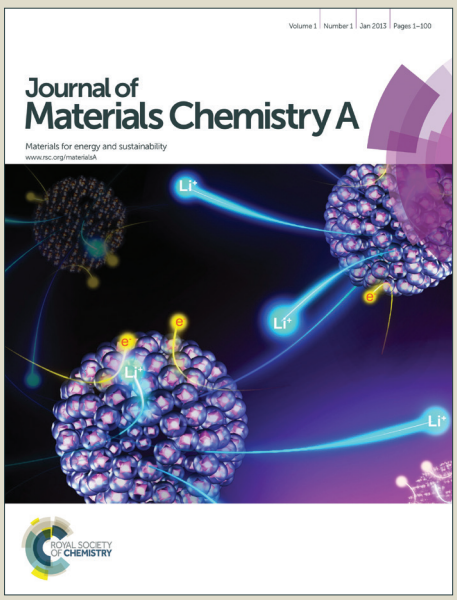

ROYAL SOCIETY OF CHEMISTRY

www.rsc.org/materialsA

Hierarchical WO_3@SnO_2 core-shell nanowire arrays on carbon cloth: a new class of anode for high-performance lithium-ion batteries

Lina Gao, Fengyu Qu, Xiang Wu*

Key Laboratory for Photonic and Electronic Bandgap Materials, Ministry of Education and College of Chemistry and Chemical Engineering, Harbin Normal University, Harbin 150025, P. R. China

We report a facile, two-step hydrothermal method to synthesize WO_3@SnO_2/carbon cloth heterostructure. Hybrid nanowire array/carbon cloth electrodes exhibit a high reversible capacity of 1000 mA h g^{-1} after 200 cycles at a current density of 0.28 C, much higher than that of the pristine WO_3 nanostructure, and enhanced rate capability at current densities ranged from 0.28 to 5 C. The superior electrochemical performances of the composite nanostructures can be ascribed to the incorporation of SnO_2, which decreases the overall battery internal resistance and improves the conductively of the composite electrodes.

Any correspondence should be addressed: E-mail:wuxiang05@gmail.com

1. Introduction

Lithium-ion batteries (LIBs), one of the most important light-weight, low-cost, highly efficient and environmentally friendly rechargeable power sources for consumer electronic products, have attracted worldwide attention due to the ever-increasing concerns about the environmental problems and limited global energy supply.[1-11] However, the search for high performance LIBs and their miniaturization never stops and there are continuous demands for the development of LIBs with higher power and energy densities.[12-15] The performances of lithium-ion batteries depend largely on the properties and structures of the electrode materials for lithium storage.[16-17] Compared to two-dimensional (2D) thin film structure, three-dimensional (3D) structures such as nanowire/nanotube arrays can potentially utilize the vertical dimension to increase the active material loading (thus the areal capacity) while maintaining similar Li ion-transport distances.[18-20]

The limited capacity and rate capability of graphite have triggered tremendous interest in research towards alternative anode materials with large capacities and good rate performance. Currently, transition metal oxides, such as tungsten trioxide, have recently become a hotspot as the anode materials to replace the commercial carbon-based materials for LIBs and exhibited high reversible capacity resulting from their unique electrochemical conversion process.[21-23] However, tungsten trioxide still suffers from poor capacity retention due to the low conductivity and large volume swings during charge/discharge cycling. To alleviate the mechanical strain/stress and increase the electrical conductivity of electrodes, an approach of creating a

nanocomposite consisting of metal oxides proves to be quite efficient. SnO_2 has been considered as an important candidate for fabricating hybrid coating layer as anode material for lithium-ion batteries due to its high theoretical specific capacity (790 mA h g^{-1}) and high conductivity.[25-30]

In this paper, we develop a simple strategy to design and fabricate 3D heterostructured WO_3@SnO_2 core-shell nanowire arrays on a carbon cloth substrate via a hydrothermal method for using as binder-free 3D anode and demonstrate that the electrochemical performance of this electrode is promising for application in lithium ion batteries.[31-32] The 3D WO_3@SnO_2 nanowire array is well in contact with and strongly supported on the carbon cloth substrate, avoiding the use of polymer binder/conductive additives, and thus the inactive interface is significantly reduced. The amorphous SnO_2 are well wrapped on WO_3 nanowire surfaces, which increase the performance during the lithium ion insertion/de-insertion in the WO_3@SnO_2 nanowire arrays electrode.

2. Experimental

All reagents were of analytical grade and used without any purification. Our experiment contains two steps: the growth of WO_3 nanowire array and the fabrication of WO_3@SnO_2 core-shell nanowire array composite. The synthesis of WO_3 nanowire array on carbon cloth has been detailed in our previous report.[22] Typically, 12.5 mmol of sodium tungstate dihydrate ($Na_2WO_4 \cdot 2H_2O$) was dissolved in deionized water (100 mL) and adjusted pH value of the solution to 1.2 with 3 M hydrochloric acid aqueous solution. Then, 35 mmol oxalic acid ($H_2C_2O_4$) was added into the above mixture and

diluted to 250 mL. The above 40 mL solution was transferred into a Teflon-lined stainless autoclave (50 mL volume), and then 2 g of $(NH_4)_2SO_4$ was added to the solution. A piece of carbon cloth was put into the autoclave then sealed, and maintained at 180 °C for 16 h. After the autoclave cooled down to room temperature, the carbon cloth was taken out and rinsed with deionized water several times and dried at 60 °C in ambient air. To synthesize WO_3@SnO_2 core-shell nanowire array, the carbon cloth-supported WO_3 nanowire array was immersed into a mixture of 0.1g of $SnCl_2 \cdot 2H_2O$ and 34 ml of diluted hydrochloric acid (0.65 M). The mixture was transferred into a Teflon-lined stainless-steel autoclave and hydrothermally treated at 180 ^oC for 20 h. After the reaction was finished, the carbon cloth was taken out, washed with deionized water and ethanol, and then dried at 60 ^oC. Finally, the products were annealed at 450 ^oC for 2h.

Scanning electron microscope (SEM) images and energy dispersive X-ray spectroscopy (EDS) analyses were obtained using a Sirion 200 microscope. Transmission electron microscope (TEM) and high-resolution TEM (HRTEM) observations were carried out on a Philips CM 200 instrument. The Brunauer-Emmett-Teller (BET) surface area and porosity were determined by nitrogen-sorption using a Micromeritics APSP 2020 analyzer.

The electrochemical performance of WO_3@SnO_2 samples was measured by assembling CR2032 coin-type half cells at room temperature, which consist of a lithium foil as the counter electrode and reference electrode, the celgard 2300 as the separator membrance, and a piece of WO_3@SnO_2 carbon cloth as the working

electrode without any conductive agent or polymeric binder. The electrolyte was 1 mol L^{-1} $LiPF_6$ in a mixture of ethylene carbonate (EC) and dimethyl carbonate (DMC) (v/v = 1:1). Cell assembly was carried out in an argon-filled glove box with moisture and oxygen concentrations below 1.0 ppm. The coin cells were galvanostatically discharged/charged at different current densities between 0.01 and 3.00 V (vs.Li^{+1}/Li) by using a battery testing system (LAND, China). Cyclic voltammetry (CV) was measured on an electrochemical workstation (CHI 760D, CH Instruments Inc., Shanghai) and electrochemical impedance spectrometry was obtained in the frequency range from 100 kHz to 0.1 Hz at room temperature.

3. Results and Discussion

The WO_3@SnO_2 nanostructures were synthesized via a facile hydrothermal method combined with a post-treatment process. Figure 1 shows X-ray diffraction (XRD) pattern of the as-synthesized WO_3@SnO_2 products. All the diffraction peaks can be well-indexed to the hexagonal phase of WO_3 (JCPDS card No. 85-2460) and SnO2 crystal (JCPDS card No. 41-1445). WO_3@SnO_2 core-shell nanowire arrays composites were synthesized by deposition of amorphous SnO_2 onto the surfaces of WO_3 nanowires as illustrated in Figure 2. The amorphous SnO_2 shells will facilitate ion diffusion and provide high energy storage capacity. From Figure 3a and b, the surface of each carbon fiber is uniformly covered with WO_3 samples. Further observation finds that WO_3 nanowire arrays grow tidily and closely on the surface of the carbon microfiber. WO_3 nanowires/carbon cloth are then putted into a mixture of $SnCl_2 \cdot 2H_2O$ and diluted hydrochloric acid, after hydrothermally treated at 180 ^oC for

20 h, WO_3@SnO_2 composite are obtained. As shown in Figure 3c, d, WO_3@SnO_2 nanowires become slightly longer in length and larger in diameter after depositions of SnO_2 layer; however, the nanowire morphology is preserved uniformly.

The structure and morphology evolution of the composite array is further investigated by TEM. After deposition of the SnO_2 layer, the morphology is maintained (Figure 4a). WO_3@SnO_2 core-shell nanowire arrays are about 500 nm in length. Figure 4b shows a HRTEM image of an individual WO_3@SnO_2 core-shell nanowire. The plane spacing of lattice fringes is indexed for the h-WO_3 nanostructure. It is clear that a thin SnO_2 layer were uniformly coated on the surface of WO_3 nanowire, resulting in the formation of hybrid core-shell nanowire. EDS spectrum taken from the core-shell nanowire suggests the existence of W, O, and Sn, confirming the introduction of SnO2 layer, as demonstrated in Figure 4c.

To investigate the electrochemical performance of the 3D hybrid core-shell nanostructures, the Brunauer-Emmett-Teller (BET) surface area and porosity are first carried out by nitrogen sorption and the corresponding N_2 adsorption-desorption isotherm is shown in Figure 5. The isotherms are of type IV with a hysteresis loop at high relative pressure indicating the WO_3@SnO_2 nanowire arrays possess a large surface area. According to Figure 5, one can clearly find that the WO_3@SnO_2 nanowire arrays possess a surface area of 8.25 m^2/g, which is about ten times larger than that of carbon cloth (0.76 m^2/g) and about two times than WO_3 nanowire array (4.44 m^2/g). The enhanced surface area after coated with SnO_2 layer renders the hybrid nanostructures more active and is beneficial for providing large interface

between the electroactive materials and the electrolyte. The results indicate that WO_3@SnO_2 hybrid composite structure may display enhanced electrochemical performance of LIBs than the pure WO_3 nanostructures.[33]

The successful growth of WO_3 and WO_3@SnO_2 hybrid nanostructures with a uniform morphology on the conductive carbon cloth with high density makes it possible as a binder-free anode for LIBs without any further treatment. The electrochemical properties of the WO_3@SnO_2 hybrid electrodes were investigated by configuring them as coin-type batteries. Figure 6a and 6b show the discharge/charge voltage profiles of the WO_3 and WO_3@SnO_2 nanostructures electrodes at a current density of 0.28 C (1 C=696 mA g^{-1}) between 0.01 and 3.0 V *versus* Li^+/Li for the first cycle, respectively. In the first discharge curve of the WO_3 electrode, there are two obvious plateau at around 1.6 V and 1 V, which can be ascribed to the decomposition of WO_3 to W (eqn (1)). In the charge process, voltage slopes can be observed at 0.2-1.0 V, which is associated with the oxidation of W back to W^{6+} (eqn (2)). WO_3 and WO_3@SnO_2 hybrid nanostructures electrodes deliver large initial discharge capacity of 1220 and 1900 mAh g^{-1} during the first cycle, respectively, which may be attributed to form of the solid electrolyte interface (SEI) layer and the decomposition of the electrolyte. [34-36]

$$WO_3 + 6Li^+ + 6e^- \rightarrow W + 3Li_2O \quad (1)$$

$$W + 3Li_2O \rightarrow WO_3 + 6Li^+ + 6e^- \quad (2)$$

No significant difference of the voltage profiles between the WO_3 and the hybrid electrodes indicate that the reaction between the introduced SnO_2 and lithium

is too feeble to contribute to the total capacity of WO_3@SnO_2 electrode.[37]

Stable cyclic performance of electrode materials is important for the practical application of lithium-ion batteries. Figure 6c displays discharge/charge capacity *versus* cycle number curves from the first cycle to the 200th cycle of WO_3 and WO_3@SnO_2 nanostructures electrodes at a current density of 0.28 C between 0.01 and 3.0 V. It is observed that the composite electrode shows considerable enhanced discharge/charge capacity with respect to the pure WO_3 electrode during all the 200 cycles. The WO_3@SnO_2 nanostructures electrodes exhibits a discharge capacity of 1100 mAh g^{-1} during the 10 th cycle and remains at 1000 mAh g^{-1} after 200 cycles, which are higher than those of the pure the WO_3 electrode (650, and 220 mAh g^{-1} during the 10 th and after 200 cycles, respectively). It can be see that the specific capacities of WO_3@SnO_2 nanostructures electrodes higher than the theoretical value. The increasing specific capacity for WO_3@SnO_2 nanostructures electrodes may be ascribed to the reversible growth of a polymeric gel-like film resulting from kinetically activated electrolyte degradation.[5,38-39] Furthermore, the hybrid electrode exhibits excellent cycling performance especially after 150 cycles, compared with the pure WO_3 electrode, because to some extent , the introduced SnO_2 layer can prevent the electrode from volume swings during charge/discharge cycles. To better understand the advantage of the WO_3@SnO_2 nanostructures in lithium storage, the rate performance of the WO_3@SnO_2 nanostructures electrode is also investigated (Figure 6d). Obviously, compared with the pristine WO_3 electrode, the specific capacities of the composite electrode are substantially increased at all investigated

discharge/charge rates at current densities of 0.28 C, 1 C, 2 C, 3 C and 5 C. It depicts that the discharge capacity are around 1100, 917, 718, 590 and 445 mAh g^{-1} after 10 cycles at current densities of 0.28, 1, 2, 3 and 5 C, respectively, which are higher than those of the pristine WO_3 electrode (550, 331, 208, 133 and 70 mAh g^{-1}). The improved rate performance of the hybrid electrode can be ascribed to the enhanced conductivity of the core-shell nanostructures after coated with SnO_2 layer. These results reveal that the incorporation of SnO_2 into WO_3 nanostructures can greatly enhance the electrochemical performance for lithium storage.

The battery after cycle has placed for one month to investigate the stability of WO_3@SnO_2 hybrid nanostructures electrode. The composite electrode is further cycled at increasing humidity of 50, 70, and 90% for 10 cycles, respectively in Figure 7a. The current densities for all cycles are kept constant at 0.28 C. The dependence of charge/discharge capacities versus humidity is summarized. The capacity can remain a stable cyclable stage during 30 cycles at different humidity. The result exhibits the perfect stability and recyclability when applying in the special conditions. To gain further insight into the enhanced electrochemical behaviors of the hybrid electrode, electrochemical impedance spectroscopy measurements are carried out on WO_3 and WO_3@SnO_2 nanostructures electrodes at room temperature, as shown in Figure 7b. An equivalent circuit (Figure 7b, inset) is used for fitting the electrochemical impedance spectra. The intercept at the Z_{real} axis at high frequency corresponds to the ohmic resistance (R_e), which represents the total resistance of the electrolyte, separator, and electrical contacts. The semicircle in the low frequency range indicates

the charge transfer resistance (R_{ct}) and constant phase element of electrode/electrolyte interface (CPE). The inclined line at lower frequency represents the Warburg impedance (W) corresponding to lithium-ion diffusion process. The resistance of the combination of the electrolyte, separator, and electrical contacts (R_e) is similar for both electrodes. This is because these binder-free, self-supported, 3D nanowire-carbon textile electrodes induce good conductivity. It can be clearly seen that the fitted value of R_{ct} is much smaller for the WO_3@SnO_2 electrode (R_{ct}=58 Ω) than for the WO_3 electrode (R_{ct}=71 Ω), which indicates that the introduction of SnO_2 enable much easier charge transfer at the electrode/electrolyte interface, and consequently decrease the overall battery internal resistance, resulting in significant improvement in the electrochemical performances.[40]

4. Conclusions

In summary, WO_3@SnO_2 hybrid nanowires/carbon cloth has been fabricated by a facile hydrothermal process and a subsequent solution reaction. This composite delivers a high reversible capacity of 1000 mA h g^{-1} after 200 cycles at a current density of 0.28 C and exhibits enhanced rate capability at current densities ranged from 0.28 to 5C. The superior electrochemical performances of the composite nanostructures can be ascribed to the incorporation of SnO_2, which decreases the overall battery internal resistance, improves the conductively of the composite electrodes, and stabilizes the WO_3 nanostructures. Thus, this composite is a promising potential anode material for lithium-ion batteries. Further rational design and development of novel hierarchical transition metal oxide heterostructures will open up

more new research opportunities in a variety of applications, such as photoconversion, sensing and electrochemical energy storage.

Acknowledgements

This work was supported Program for New Century Excellent Talents in Heilongjiang Provincial University (1252-NCET-018)

References

1. M. Armand and J. M. Tarascon, *Nature*, 2008, **451**, 652-657.
2. Y. T. Han, X. Wu, Y. L. Ma, L. H. Gong, F.Y. Qu and H. J. Fan *CrystEngComm.*, 2011, **13**, 3505-3510.
3. P. Poizot and F. Dolhem, *Energy Environ. Sci*., 2011, **4**, 2003-2019.
4. L. W. Ji, Z. Lin, M. Alcoutlabi and X. W. Zhang, *Energy Environ. Sci*., 2011, **4**, 2682-2699.
5. B. Liu, J. Zhang, X. F. Wang, G. Chen, D. Chen, C.W. Zhou, and G .Z. Shen, *Nano Lett*.,2012, **12**, 3005-3011.
6. B. Liu, X. F. Wang, H. T. Chen, Z. R. Wang, D. Chen, Y. B. Cheng, C. W. Zhou and G. Z. Shen, *Scientific Reports*, 2013, **3**, 1622-1668.
7. J.Yan, A.Sumboja, E. Khoo and P. S. Lee, *Adv. Mater*., 2011, **23**, 746-750.
8. S. Venkatachalam, H. W. Zhu, C. Masarapu, K. H. Hung, Z. Liu, K. Suenaga and B. Q. Wei, *ACS Nano*, 2009, **3**, 2177-2184.
9. S. J. Ding, J. S. Chen, and X. W. Lou, *Adv. Funct. Mater*., 2011, **21**, 4120-4125.
10. S. H. Liu, Z. Y. Wang, C. Yu, H. B. Wu, G. Wang, Q. Dong, J. S. Qiu, A. Eychmüller, and X. W. Lou, *Adv. Mater*., 2013, **25**, 3462-3467.
11. Y. Wang, Z. S. Feng, J. J. Chen, C. Zhang, X. Jin, J. Hu, Solid State Commun., 2012,**152**,1577-1580.
12. K. S. Kang, Y. S. Meng, J. Breger, C. P. Grey and G. Ceder, *Science*, 2006,**311**, 977-980.
13. H. B. Wu, J. S. Chen, H. H. Hng and X. W. Lou, *Nanoscale*, 2012, **4**, 2526-2542.

14. G. Derrien, J. Hassoun, S. Panero and B. Scrosati, *Adv. Mater.*,2007,**19**, 2336-2340.

15. J. Jiang, Y. Y. Li, J. P. Liu, X. T. Huang, C. Z. Yuan and X. W. Lou, *Adv. Mater.*, 2012, **24**, 5166-5180.

16. H. G. Wang, D. L. Ma, X. L. Huang, Y. Huang and X. B. Zhang, *Sci. Rep*. 2012, **2**, 481-488.

17. X. F. Wang, B. Liu, Q. F Wang, W. F. Song, X. J Hou, D. Chen, Y. B. Cheng, G. Z. Shen, *Adv. Mater.*, 2013, **25**, 1479-1486.

18. J. P. Liu, J. Jiang, C. W. Cheng, H. X. Li, J. X. Zhang, H. Gong, H. J. Fan, *Adv. Mater.*, 2011, **23**, 2076-2081.

19. J. Bae, M. K. Song, Y. J. Park, J. M. Kim, M. L. Liu and Z. L. Wang, *Angew. Chem*., Int. Ed., 2011, **50**, 1683-1687.

20. Y. S. Luo, J.S. Luo, J. Jiang, W. W. Zhou, H. P. Yang, X.Y. Qi, H. Zhang, H. J. Fan, D. Y. W. Yu, C. M. Li and T. Yu, *Energy Environ. Sci*., 2012, **5**, 6559-6566.

21. J. Q. Yang, L. F. Jiao, Q. Q. Zhao, Q. H. Wang, H. Y. Gao, Q. N. Huan, W. J Zheng, Y. J. Wang and H. T. Yuan, *J. Mater. Chem*., 2012, **22**, 3699-3701.

22. L. N. Gao, X. F Wang, Z. Xie, W. F. Song, L. J. Wang, X. Wu, F. Y. Qu, D. Chen and G. Z Shen, *J. Mater. Chem. A*, 2013, **1**, 7167-7173.

23. W. J. Li and Z. W. Fu, *Appl. Surf. Sci*., 2010, **256**, 2447-2452.

24. S. Yoon, E. Kang, J. K. Kim, C. W. Lee and J. Lee, *Chem. Commun*., 2011, **47**, 1021-1023.

25. W. W. Zhou, C. W. Cheng, J. P. Liu, Y. Y. Tay, J. Jiang, X. T. Jia, J. X. Zhang, H.

Gong, H. H. Hng, T. Yu and H. J. Fan, *Adv. Funct. Mater.*, 2011, **21**, 2439-2445.

26. X. M. Wu, S. C. Zhang, L. L. Wang, Z. J. Du, H. Fang, Y. H. Ling and Z. H. Huang, *J. Mater. Chem.*, 2012, **22**, 11151-11158.
27. X. Y. Xue, Z. H. Chen, L. L. Xing, S. Yuan and Y. J. Chen, *Chem. Commun.*, 2011,**47**, 5205-5207.
28. X. Y. Xue, B. He, S. Yuan, L. L. Xing, Z. H. Chen and C. H. Ma, Nanotechnology 2011, 22, 395702.
29. S. J. Ding, J. S. Chen, G. G. Qi, X. N. Duan, Z. Y. Wang, E. P. Giannelis, L. A. Archer, and X. W. Lou, J. Am. Chem. Soc. 2011, 133, 21-23.
30. C. Yue, Y. J. Yu, J. Yin, T. L. Wong, Y. S. Zang, J. Li and J. Y. Kang, *J. Mater. Chem. A*, 2013, **1**, 7896-7904.
31. X. F. Wang, B. Liu, Q. Xiang, Q. Wang, X. Hou, D. Chen, G. Z. Shen. ChemSusChem 2014, 7, 308-313.
32. X.. F. Wang, B. Liu, R. Liu, Q. Wang, X. Hou, D. Chen, R. Wang, G. Z. Shen, Angew. Chem. Int. Ed. 2014, 53, 1849-1853.
33. Y. L. Wang, J. J. Xu, H. Wu, M. Xu, Z. Peng and G. F. Zheng, *J. Mater. Chem.*, 2012, **22**, 21923-21927.
34. Y. Qi, N. Du, H. Zhang, X. Fan, Y. Yang and D. R. Yang, *Nanoscale*, 2012, **4**, 991-996.
35. Y. C. Qiu, G. L. Xu, Q. Kuang, S. G. Sun, and S. H. Yang, *Nano Res.*, 2012, **5**, 826-832.
36. Z. Y. Wang, D.Y. Luan, F. Y. C. Boey, and X. W. Lou, J. Am. Chem. Soc. 2011,

133, 4738-4741.

37. X. F. Wang, Q. Y. Xiang, B. Liu, L. J. Wang, T. Luo, D. Chen & G. Z. Shen, *Sci. Rep.*, 2013, **3**, 2007-2014.

38. X. H. Wang, X. W. Li, X. L. Sun, F. Li, Q. M. Liu, Q. Wang and D. He, *J. Mater. Chem*., 2011, **21**, 3571-3573.

39. G. M. Zhou, D.W. Wang, F. Li, L. L. Zhang, N. Li, Z. S. Wu, L. Wen, G. Q. Lu, and H. M. Cheng, *Chem. Mater.*, 2010, **22**, 5306-5313.

40. Y. Wang, Z. S. Feng, C. Zhang, L. Yu, J. J. Chen, J. Hu and X. Z. Liu, Nanoscale, 2013, 5, 3704–3712.

Figures Caption

Figure 1. XRD patterns of WO_3@SnO_2 composites; standard data of SnO_2 (red line) and WO_3 (blue line).

Figure 2. Schematic of the synthesis procedure of WO_3@SnO_2 composite nanowire arrays on carbon cloth.

Figure 3. (a,b) SEM images of WO_3 nanowires grown on carbon cloth. (c,d) SEM images of WO_3@SnO_2 nanowires grown on carbon cloth.

Figure 4. (a,b) TEM images and (c) EDS pattern of WO_3@SnO_2 core-shell nanowire arrays.

Figure 5. N_2 adsorption-desorption isotherm of the samples. (a).pure carbon cloth. (b) WO_3 nanowire arrays. (c) WO_3@SnO_2 composites.

Figure 6. Discharge/charge voltage profiles of (a) WO_3, and (b) WO_3@SnO_2 hybrid nanostructures electrodes. Comparison of the cycling performance of WO_3 and WO_3@SnO_2 nanostructures electrodes: (c) at 0.28 C, and (d) at various current densities of 0.28, 1, 2, 3, and 5 C.

Figure 7. (a) Stability test of WO_3@SnO_2 nanostructures electrode at various humidity of 50, 70, and 90%. (b) Electrochemical impedance spectra of WO_3 and WO_3@SnO_2 nanostructures electrodes, with the inset showing the equivalent circuit.

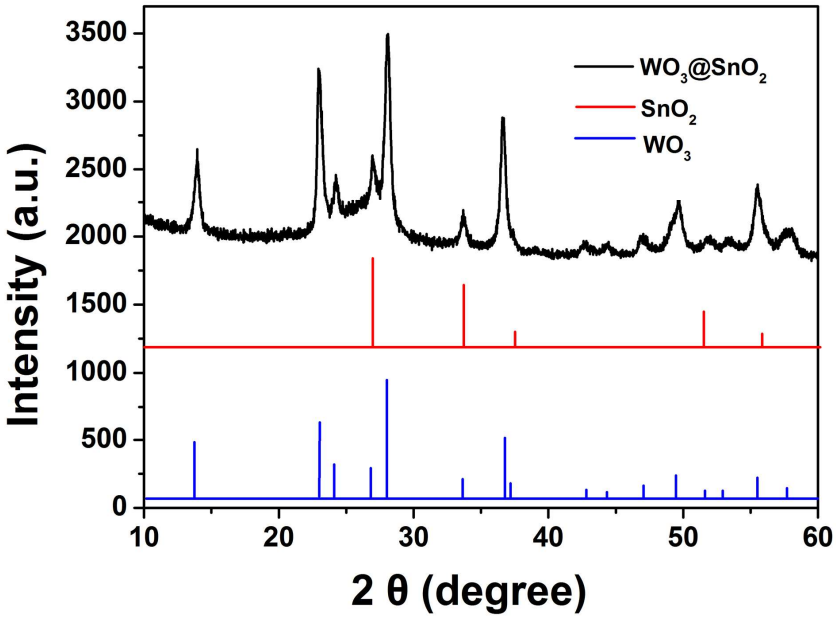

Figure 1 Lina Gao et al.

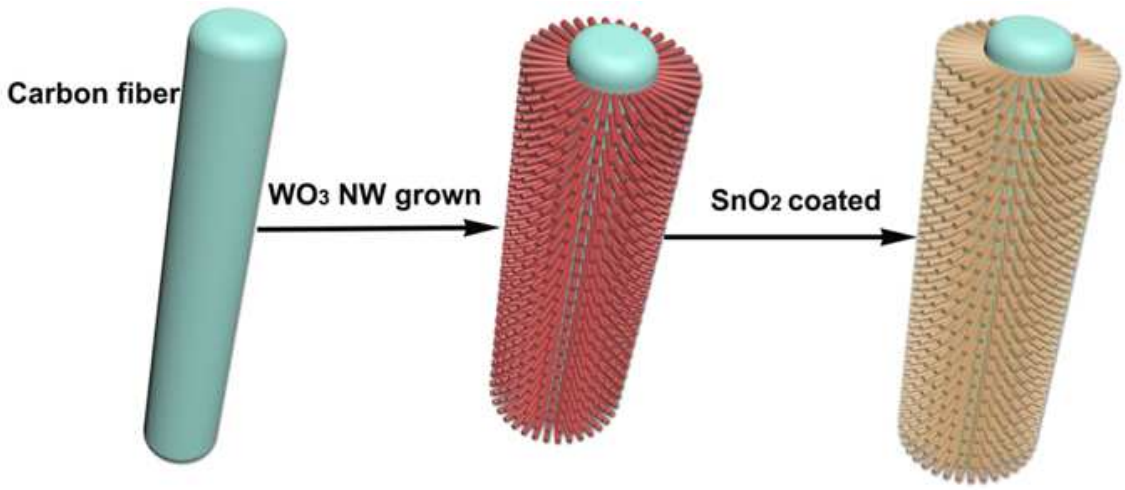

Figure 2 Lina Gao et al.

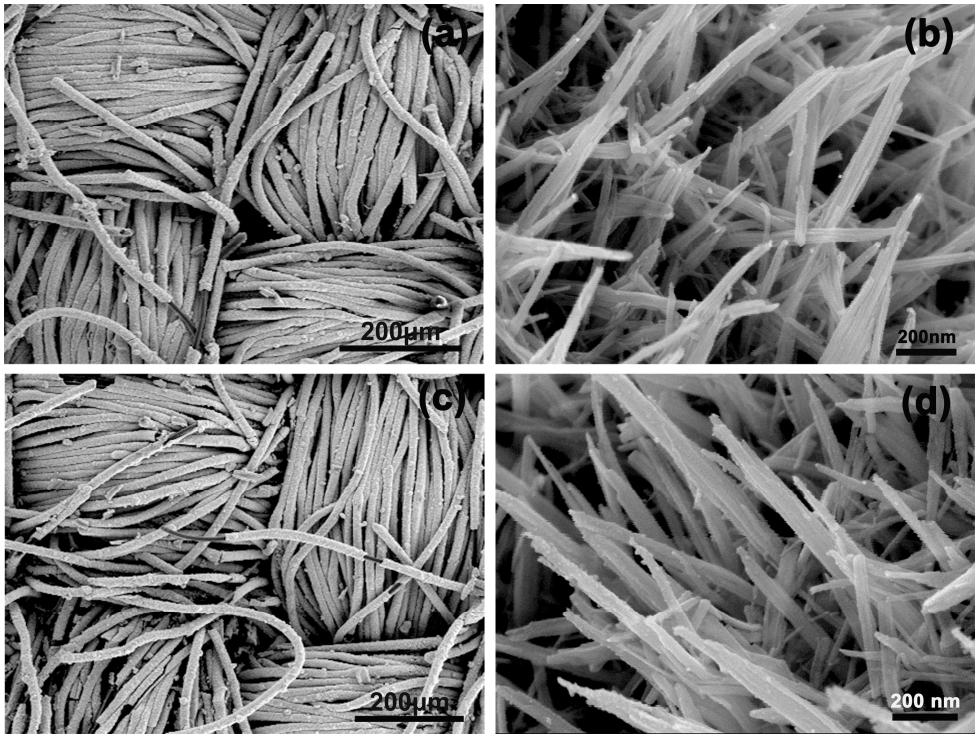

Figure 3 Lina Gao et al.

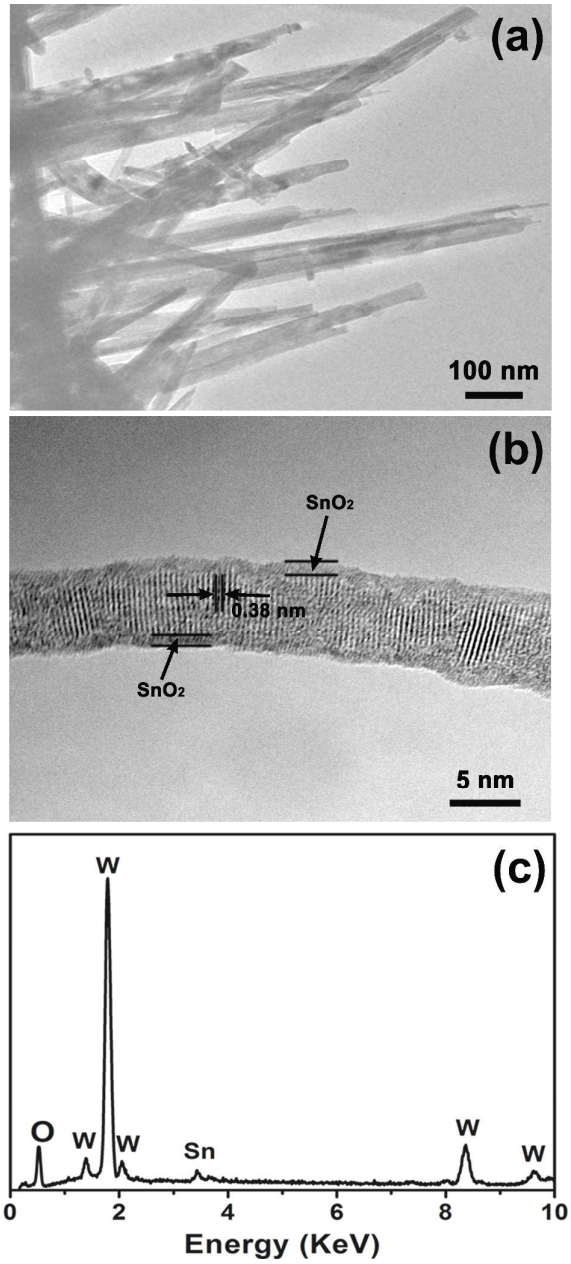

Figure 4 Lina Gao et al.

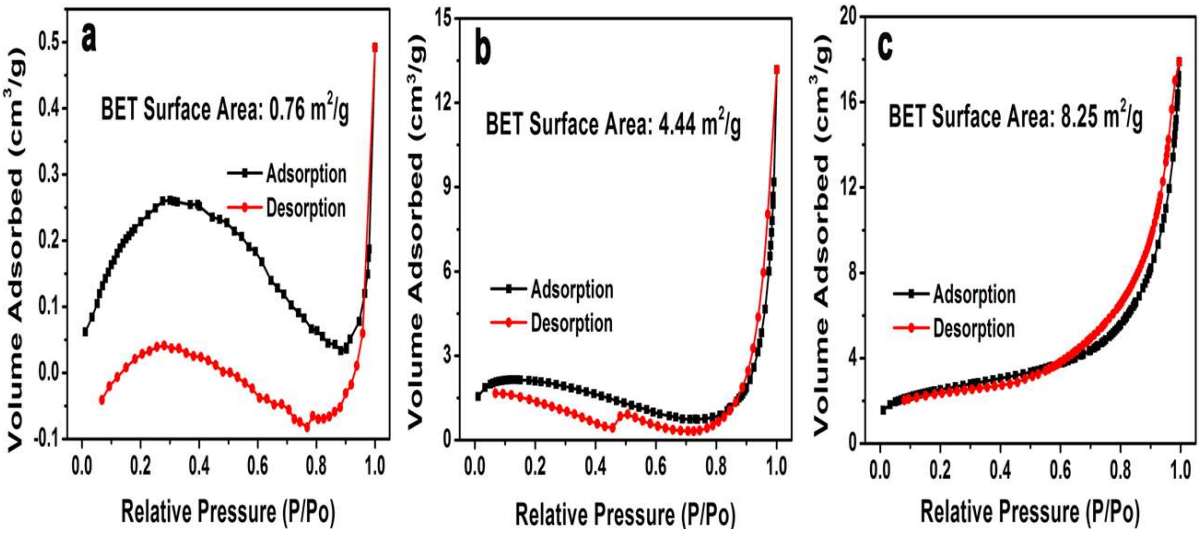

Figure 5 Lina Gao et al.

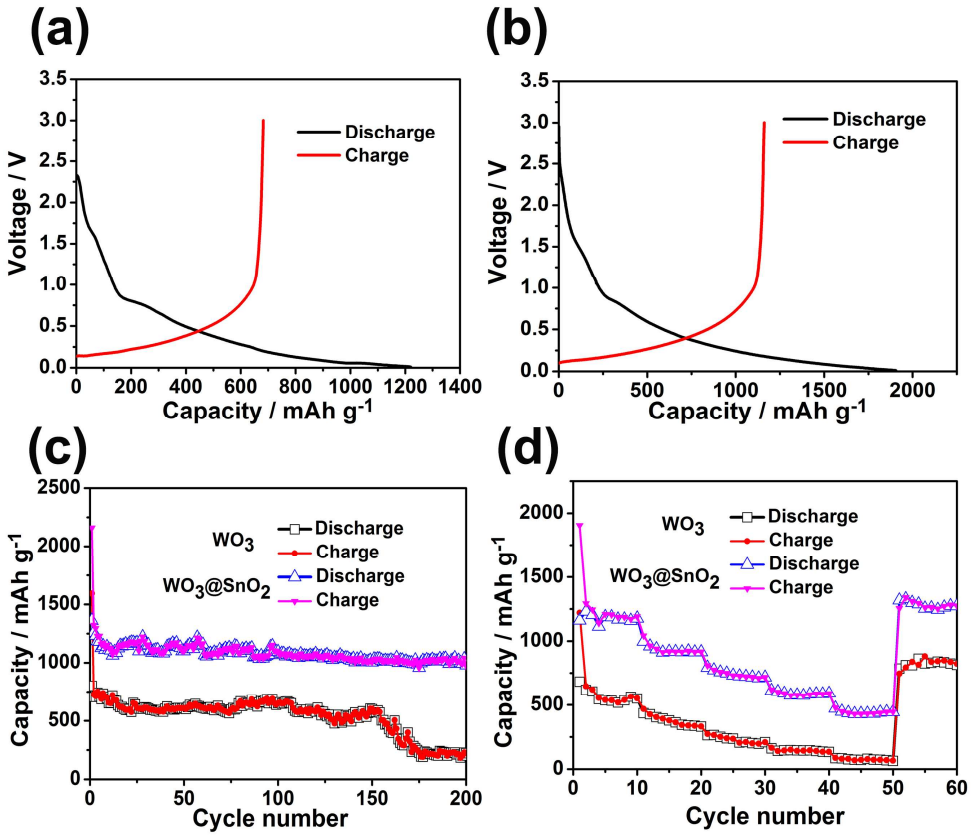

Figure 6 Lina Gao et al.

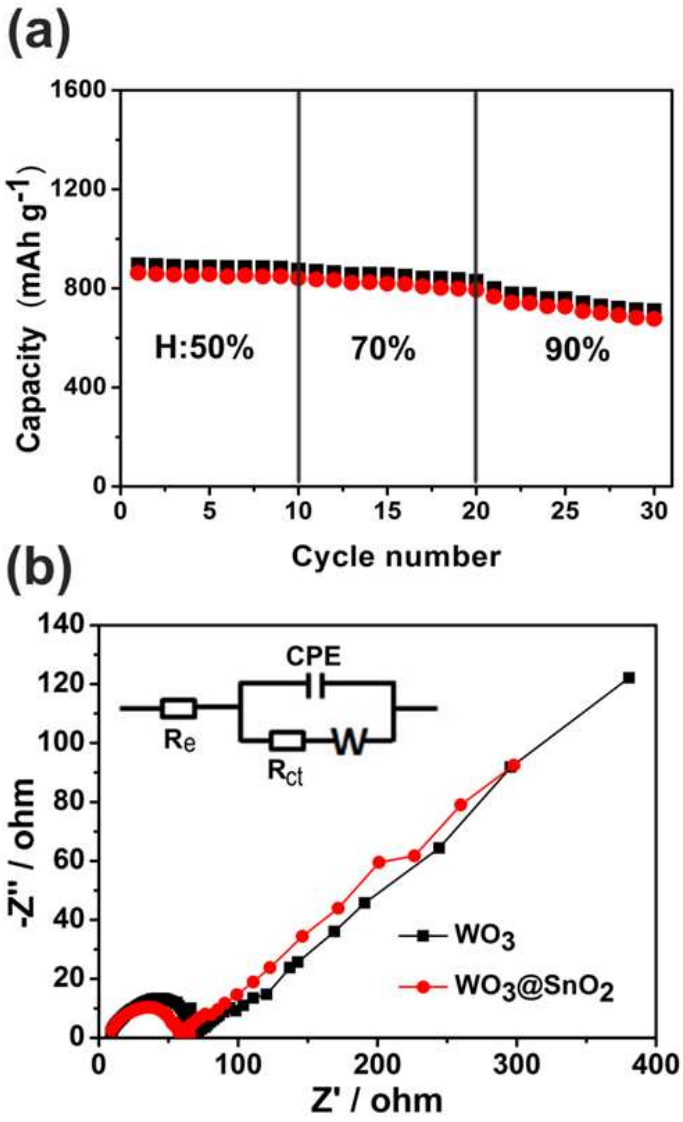

Figure 7 Lina Gao et al.

Graphical Abstract

Hybrid WO_3@SnO_2 nanowire array/carbon cloth electrodes exhibit a high reversible capacity of 1000 mA h g^{-1} after 200 cycles. The superior electrochemical performances of the composite can be ascribed to the incorporation of SnO_2, which decreases the overall battery internal resistance and improves the conductively of the composite electrodes.